JOURNAL OF COMPUTATIONAL PHYSICS 63, 85–106 (1986)

The Random Choice Method Applied to Two-Dimensional Shock Focusing and Diffraction

H. OLIVIER AND H. GRÖNIG

Stosswellenlabor, Rheinisch-Westfälische Technische Hochschule Aachen, Templergraben 55, Aachen 5100, West Germany

Received June 6, 1984; revised February 15, 1985

After a brief introduction to the Random Choice Method (RCM) of one space dimension and a short discussion of some of its essential features an application to two space dimensions is made, based on an operator splitting technique proposed by Chorin. To show the influence of the random number generators, results are presented using both a generator proposed by Chorin and that of van der Corput. As a numerical test problem, the shock focusing by a concave reflector is calculated. The numerical results are compared with experimental ones. For the first time the agreement between the numerical and experimental results is quite good using the RCM in two space dimensions. Furthermore the application of the RCM to shock diffraction at a 90° corner is shown. These results are also compared with experimental ones. © 1986 Academic Press, Inc.

1. INTRODUCTION

During the past years several numerical methods have been applied to the solution of flow problems in unsteady gas dynamics involving shock and rarefaction waves and contact surfaces. These methods are usually based on finite-difference schemes. Unfortunately most of these methods produce oscillations behind discontinuities, and due to numerical diffusion low resolution results are obtained in continuous parts of the flow.

The development of the one-dimensional RCM by Glimm (5), Chorin (1), and Sod (9) has made it possible to overcome the difficulties caused by numerical oscillation and diffusion. This method was first used by Glimm (5) as part of a proof of existence of solutions to systems of nonlinear hyperbolic conservation equations. Chorin (1, 2) applied the RCM to problems of gas dynamics giving a short introduction to its application to multidimensional problems. Based on this concept, this method is applied to two-dimensional problems in this paper. Although one computes solutions on a grid with Glimm's method it does not represent a difference method, which usually computes a weighted sum to obtain the value of the solution at a specific grid point. The RCM samples values from an explicit wave solution. Due to this sampling in one space dimension no smoothing of discontinuities appears.

0021-9991/86 $3.00
Copyright © 1986 by Academic Press, Inc.
All rights of reproduction in any form reserved.

The advantages of the one-dimensional RCM in comparison with finite difference methods are:

(i) Discontinuities as shocks or contact surfaces are computed without numerical diffusion and dispersion.

(ii) There are no numerical oscillations behind discontinuities.

(iii) Boundary conditions are readily handled.

The disadvantages of the RCM in comparison with finite difference methods are:

(i) Due to the randomness the profile of a rarefaction wave is not computed smooth but on the average very close to the exact solution.

(ii) The locations of discontinuities at any time are not exact, however, their average positions are.

The main attention in this paper is drawn to the application of the RCM to flow problems in two space variables. Since the two-dimensional method is based on the one-dimensional, in Section 2 an outline of the RCM in one space dimension is presented. The solution of the inherent Riemann problem and the sampling procedure are not described, since those may be found in Chorin's papers (1, 2) and other literature concerning the RCM (3, 7, 9).

In Section 3 the application to two space variables is shown. In Section 4 two families of random number generators are introduced. Some statistical quantities of these generators are compared. In Section 5 calculations are shown, which are compared with experimental results. The numerical results are discussed with respect to different conditions like different number of grid points, different random number generators, or different determination of the passive velocities.

2. RCM for One Space Dimension

2.1. *General description of* RCM

The equations for an inviscid, non-heat-conducting, one-dimensional flow may be written in the following form (1):

$$W_t + F(W)_x = 0, \tag{2.1}$$

where

$$W = \begin{pmatrix} \rho \\ m \\ e \end{pmatrix} \quad \text{and} \quad F(W) = \begin{pmatrix} m \\ m^2/\rho + p \\ m(e+p)/\rho \end{pmatrix} \tag{2.2}$$

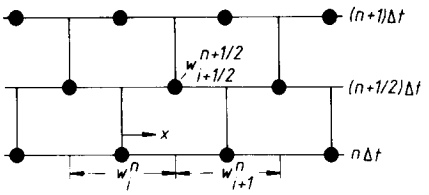

FIG. 1. Grid configuration in one space dimension.

$m = \rho u$ indicates the momentum per unit volume with the density ρ and the velocity u. The total energy per unit volume e may be written as

$$e = \rho\,\varepsilon + \tfrac{1}{2}\rho\,u^2 \tag{2.3}$$

with internal energy ε.

Δt and Δx are time and spatial increments of the used grid. One wishes to obtain solutions at the grid points $(i\Delta x, n\Delta t)$. Of course the method produces no exact solutions but only approximate ones w_i^n. The solution of the vector $W(i\Delta x, n\Delta t)$ is then approximated by $w_i^n \approx W(i\Delta x, n\Delta t)$ and analogous $w_{i+1/2}^{n+1/2} \approx W((i+1/2)\,\Delta x, (n+1/2)\,\Delta t)$. The task is to compute the solution $w_{i+1/2}^{n+1/2}$ if w_i^n and w_{i+1}^n are given. This problem can be solved if the initial data are given in the following way:

$$W(x, n\Delta t) = \begin{cases} w_{i+1}^n, & x \geqslant (i+1/2)\,\Delta x \\ w_i^n, & x < (i+1/2)\,\Delta x. \end{cases} \tag{2.4}$$

With (2.4) one sees, that the initial data are piecewise constant and discontinuous (see Fig. 1). Equation (2.1) together with (2.4) describes a Riemann problem; x is a spatial coordinate, which starts from every grid point (see Fig. 1). In the (x, t) plane the solution of the Riemann problem yields up to four regions, in which $W(x, t)$ is constant (Fig. 2). These four regions are connected by three waves: a backward and forward facing wave, i.e., either a shock or an expansion wave, and a contact discontinuity. The contact discontinuity divides S_* into two regions with different densities ρ_{*l}, ρ_{*r} and specific heat ratios γ_l, γ_r. The values of u_* and p_* are equal across the contact surface.

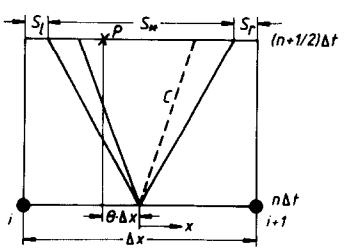

FIG. 2. Riemann problem (c = contact surface).

The solution of the Riemann problem is characterized by $W(x, t)$. Let θ_n be a value of the random variable θ equidistributed in $[-1/2, 1/2]$. Then $w_{i+1/2}^{n+1/2}$ is defined by the solution of the Riemann problem at a point $\{(i+1/2+\theta_n)\,\Delta x,\ (n+1/2)\,\Delta t\}$, i.e.,

$$w_{i+1/2}^{n+1/2} = W\{(i+1/2+\theta_n)\,\Delta x,\ (n+1/2\,\Delta t\}. \tag{2.5}$$

Equation (2.5) is the essence of the RCM. This procedure is shown in Fig. 3 graphically. P indicates the sampling point. It is important, that the waves from adjacent Riemann problems do not intersect, otherwise the described method yields no correct solution. A condition on Δt which guarantees no wave intersection is the Courant–Friedrichs–Lewy condition

$$\Delta t = \sigma\,\Delta x / \sup_i\,(|u_i^n| + c_i^n) \tag{2.6}$$

with

$$\sigma \leqslant \tfrac{1}{2};$$

c_i is the sound speed and u_i the fluid velocity at a grid point i. Godunov's iterative method to solve the Riemann problem and the sampling procedure can be found in Chorin's papers (1, 2).

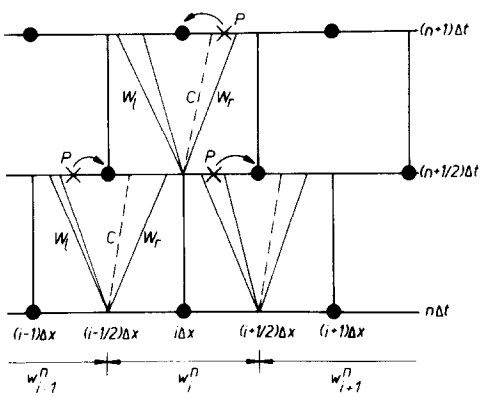

FIG. 3. Sampling procedure and grid configuration.

2.2. *Boundary Conditions*

To satisfy the solid-wall boundary conditions (Fig. 4) at time $n\Delta t$ the following conditions are imposed on a pseudo left grid point

$$\begin{aligned} p_l &= p_r, \\ \rho_l &= \rho_r, \\ u_l &= -u_r, \\ \gamma_l &= \gamma_r. \end{aligned} \tag{2.8}$$

Since in the second half-step the solution is sampled between the points $i+1/2$ and $i-1/2$ one needs no boundary conditions. Only in the first step they are imposed. In this manner waves can be reflected at a solid boundary.

3. RCM for Two Space Dimensions

Chorin (1) proposed a method for computing multidimensional unsteady compressible flows using Glimm's method by means of operator splitting. The equations of motion for an inviscid, non-heat-conducting fluid in two space dimensions are

$$\rho_t + (\rho u)_x + (\rho v)_y = 0, \tag{3.1a}$$

$$(\rho u)_t + (\rho u^2 + p)_x + (\rho uv)_y = 0, \tag{3.1b}$$

$$(\rho v)_t + (\rho uv)_x + (\rho v^2 + p)_y = 0, \tag{3.1c}$$

$$e_t + ((e+p)\,u)_x + ((e+p)\,v)_y = 0, \tag{3.1d}$$

with u and v representing the x and y component of the velocity. The energy per volume e can be expressed as

$$e = \rho\varepsilon + \frac{\rho}{2}(u^2 + v^2) \tag{3.2}$$

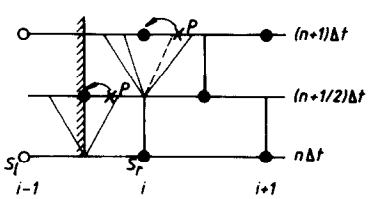

FIG. 4. Treatment of boundaries.

with the internal energy for an ideal gas

$$\varepsilon = \frac{1}{\gamma - 1} \frac{p}{\rho}. \tag{3.3}$$

The basic procedure is the use of Glimm's algorithm as a building block in a fractional step method. At each time-step four quarter-steps are performed; each quarter-step represents a sweep in either the x or y direction. When (3.1) is written for $y = \text{const}$ (x sweep)

$$\rho_t + (\rho u)_x = 0, \tag{3.4a}$$

$$(\rho u)_t + (\rho u^2 + p)_x = 0, \tag{3.4b}$$

$$(\rho v)_t + (\rho uv)_x = 0, \tag{3.4c}$$

$$e_t + ((e + p)\, u)_x = 0, \tag{3.4d}$$

and similar for $x = \text{const.}$, one sees that these two systems of differential equations are coupled by u and v.

Using (3.4a), (3.4c) can be written in the following form:

$$v_t + u\, v_x = 0. \tag{3.5}$$

Equation (3.5) says that in the x sweep v is transported as a passive scalar along the characteristic u. So we have a tool to determine the passive velocities. In the following "passive velocity" describes the component of the velocity which is normal to the computational direction, i.e., during the computation in the x direction (x sweep) v is the passive velocity and during the computation in the y direction (y sweep) u is the passive velocity. Using (3.5) we take $\bar{v} = v_l$ (y component of the velocity at the left grid point) when the sampling point is to the left of the contact surface and $\bar{v} = v_r$ when the sampling point is to the right of the contact surface for example during an x sweep, where $\bar{v}$ indicates the sampled solution of the velocity in the y direction of the Riemann problem.

At each partial step, the solution vector is approximated by a piecewise constant vector. In the x sweeps the resulting waves in the x direction are found using the one-dimensional method as described in Section 2. In the y sweeps the waves in the y direction are found again with the one-dimensional method but with u replaced by v.

The remaining task is to combine the fractional steps in such a way that in the mean the interaction of the x and y waves is properly accounted for. This is done in the following way (Chorin (1)). At the beginning of the time step ρ, p, u, v, and γ are known at points $(i\Delta x, j\Delta x)$ (Fig. 5). Then a first x sweep computes the solutions at points $(i + 1/2)\,\Delta x$ for all j. These solutions are used as initial data for the first y sweep. One obtains the solutions at points marked by 0 (Fig. 5). After the first y sweep the first half time-step is finished. The duration of the first half time-step is

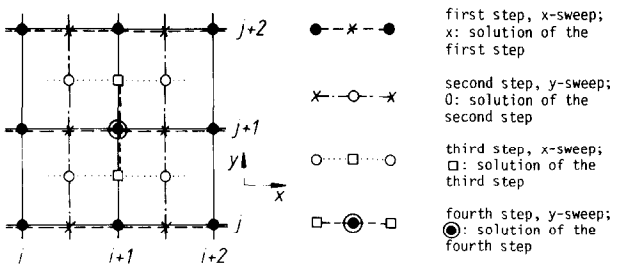

FIG. 5. Grid configuration. First step, x sweep; (x) solution of the first step. Second step; y sweep; (0) solution of the second step. Third step, x sweep; (□) solution of the third step. Fourth step, y sweep; ($\odot$) solution of the fourth step.

determined at the beginning of the first x sweep by (2.6). The y sweep is simultaneous to the former x sweep. At the beginning of the third step again (2.6) is used to determine the duration of the second half time-step. As initial conditions the solutions of the second step are used. The second x sweep or third step yields the solution at points $(j+1/2)\,\Delta x$ for all i. After the last step, an y sweep, the solution at the grid points $(i\Delta x, j\Delta x)$ is obtained.

4. USED RANDOM NUMBER GENERATORS

Chorin (1) proposed a random number generator which works with a standard deviation reduction technique as follows. Let $m_1, m_2 > m_1$ be two mutually prime integers. Consider the sequence of integers

$$n_{i+1} = (m_1 + n_i) \pmod{m_2}$$

with given $n_0 < m_2$. θ_i is a pseudo random number equidistributed over $[-1/2, 1/2]$ as uniform as possible. This random number is usually generated by a computer-installed subroutine. Then a modified sequence θ_i' of random numbers is used

$$\theta_i' = ((n_i + \theta_i + \tfrac{1}{2})/m_2) - \tfrac{1}{2}. \tag{4.1}$$

Chorin (1) mentioned, that the standard deviation of the shock position is proportional to $(1/m_2)^{1/2}$. For $m_2 \to \infty$ the standard deviation would become zero. But furthermore Chorin (1) mentioned that m_2 cannot be made too large, otherwise it introduces a systematical error into the calculation. Colella (3) used a general form of the van der Corput random generator. Let $k_1, k_2 > 0$ be integers, $k_1 > k_2$ relatively prime. The (k_1, k_2) van der Corput sampling sequence a_i is given by

$$a_i = \sum_{l=0}^{m} q_l k_1^{-(l+1)}, \tag{4.2}$$

where

$$q_l = k_2 n_1 \pmod{k_1} \qquad \text{and} \qquad \sum_{l=0}^{m} n_l k_1^l = i.$$

Equation (4.2) gives a distribution in the range [0, 1].

It is very difficult to make qualitative statements of the random number generators without using physical test problems. However, there are a few statistical qualities which allow a first assessment. These qualities, for example, are the arithmetical mean value, the standard deviation, and the so-called "chi-square" statistic. In the following examples the random numbers are equidistributed in the range [0, 1]. The arithmetical mean value of optimal equidistributed random numbers in the range [0, 1] is 0.5. The standard deviation is computed by

$$\sigma = \sqrt{(1/(N-1)) \sum_{i=1}^{N} (x_i - \bar{x})^2} \tag{4.3}$$

if

$$\bar{x} = \frac{1}{N} \sum_{i=1}^{N} x_i \tag{4.4}$$

is the arithmetical mean value and N random numbers are used in this test. The "chi-square" statistic gives a statement of the distribution of the random numbers. To compute the "chi-square" statistic the range [0, 1] is devided into k subintervals. Then the quantity of random numbers n_s is investigated, which fall into each subinterval, if N random numbers are considered in this test. Let p_s be the possibility that each random number falls into a subinterval, then the expected quantity of subinterval s is $p_s N$. The "chi-square" statistic is formed as follows:

$$U_r^2 = \sum_{s=1}^{k} \frac{(n_s - p_s N)^2}{p_s N}. \tag{4.5}$$

Of course, the theoretical distribution is approximated well by the random generator if U_r^2 is small. In this way the distribution of random numbers can be compared by (4.5). The generator with the smallest value U_r^2 has the best distribution. In the following these three test quantities have been applied to Chorin's and van der Corput's generator. There were 200 random numbers used, and the range [0, 1] was divided into $k = 20$ subintervals. Table I gives the obtained results.

The best arithmetical mean value gives Chorin's generator $m_1 = 3$, $m_2 = 7$, $n_0 = 5$ with $|\bar{x} - 0.5| = 2 \times 10^{-4}$. The smallest standard deviation is obtained by Chorin's generator $m_1 = 2$, $m_2 = 3$, $n_0 = 2$, and the smallest "chi-square" statistic by van der Corput's generator $k_1 = 5$, $k_2 = 3$ and $U_r^2 = 0.8$. In Section 5 several numerical solutions are compared which have been obtained with different random generators.

TABLE I

Statistical Quantities of Several Random Number Generators

	Chorin's generator (m_1, m_2)						
	(1,2) $n_0=2$	(2,3) $n_0=2$	(1,3) $n_0=2$	(1,5) $n_0=2$	(3,7) $n_0=5$	(3,5) $n_0=5$	(7,11) $n_0=2$
$\bar{x}$	0.5122	0.4933	0.4906	0.506	0.4998	0.4971	0.5009
σ	16.39	16.17	17.12	16.25	16.85	16.37	16.92
U_r^2	26.2	19.0	18.8	21.4	16.8	19.0	6.0
	van der Corput's generator (k_1, k_2)						
	(2,1)	(3,2)	(3,1)	(5,1)	(7,3)	(5,3)	(11,7)
$\bar{x}$	0.4946	0.4967	0.4946	0.4937	0.4997	0.496	0.4991
σ	16.6	16.48	16.5	16.64	16.55	16.63	16.53
U_r^2	1.5	1.0	1.0	2.6	1.0	0.8	1.0

5. Numerical Examples

In this Section the numerical results of two shock propagation problems are discussed and compared with experimental results. The first problem is the focusing of a plane shock wave by a parabolic reflector and the second the diffraction of a plane shock wave at a 90° corner. Both numerical calculations were made in two space dimensions. Regarding the focusing problem, the influence of the number of grid points, the passive velocities and the used random generator on the numerical solution are studied. All calculations were performed for air with $\gamma = 1.4$.

5.1. *Focusing of Shock Waves*

The numerical results are compared with experiments which were carried out by Sturtevant and Kulkarny (12). In the calculations their reflector no. 1 is used, a parabolic cylinder with a width of 20.32 cm, radius $R_{\min} = 6.03$ cm and angle of convergence $\alpha = 160°$ (Sturtevant, Kulkarny (12)). To compare the quality of the numerical results, pressure histories are calculated for the same four locations close to the reflector as given in the paper of Sturtevant and Kulkarny (12); the exact location of the pressure probes were based on an information of Sturtevant (11). According to this the probes closest to the focus are located in a cross section 3.2 mm downstream of the geometrical focus. The Mach number of the incident shock is 1.1. In the numerical calculations the shape of the reflector is approximated by a stepwise wall to apply the simple boundary conditions of (2.8). Because the considered flow problem is symmetrical, only the upper halfplane of the flow field is

computed. At the reflector boundary and at the axis of symmetry the reflection technique of (2.8) is applied. At the other boundaries of the grid no reflection is assumed.

5.1.1. *Influence of the number of grid points.* In these examples Chorin's generator is used with $m_1 = 3$, $m_2 = 7$, and $n_0 = 5$; the values of m_1 and m_2 are proposed by Chorin (1). Fig. 6 shows the pressure field before, at the moment of and after focusing. The shape of one half of the reflector cuts off part of the left portion of the grid with a nonreflecting flow region above. The vertical line in Fig. 6 indicates the geometrical focus. These pressure fields are quite similar for all mesh variations. In Fig. 7–9 the calculated pressure histories are compared with the experimental ones of Sturtevant and Kulkarny (12). The solid curves represent the measured pressures, the dotted ones the calculations. For location 2, closest to the focus, the maximum measured and calculated pressure are indicated on the diagrams. Since

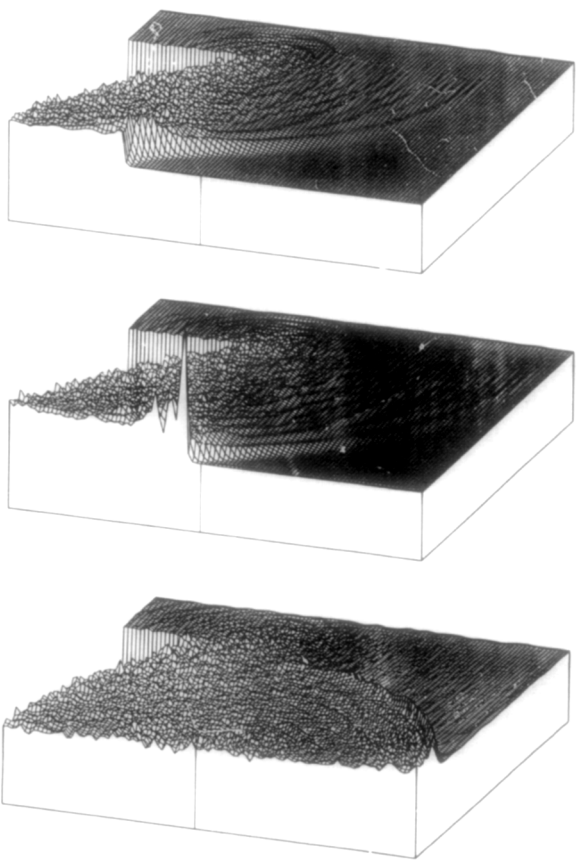

FIG. 6. Pressure field before, at and after focusing.

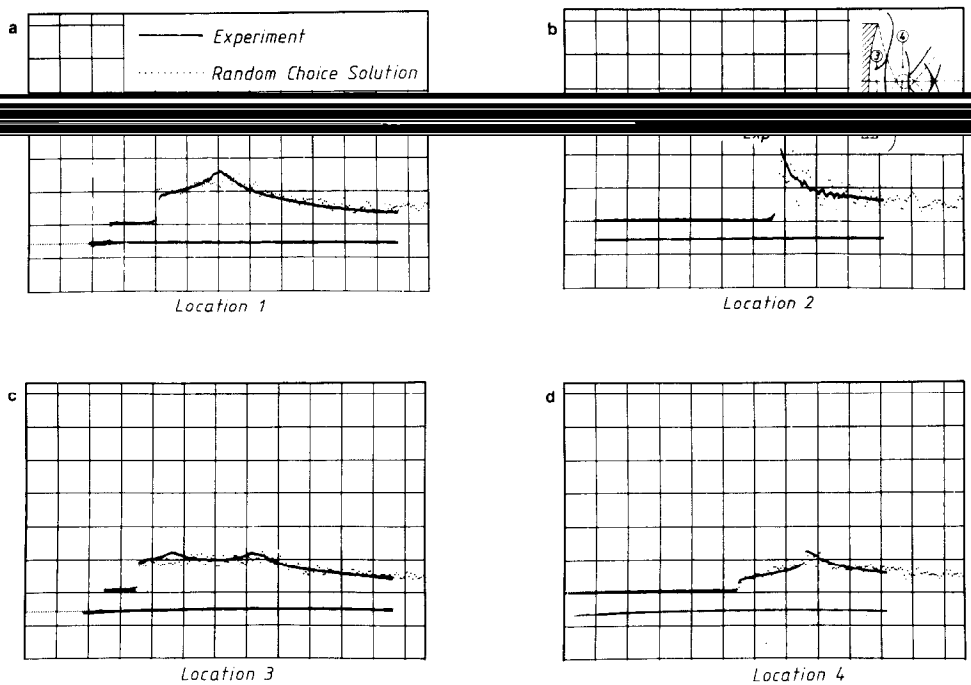

FIG. 7. Pressure histories for a 90×90 mesh. Scales: 0.4 atm/division; 0.05 ms/division.

the measured maximum pressure could not be directly read from the oscillograms this value was obtained from Fig. 9 of Sturtevant and Kulkarny (12) leading probably to a slight uncertainty. Due to the random character of the numerical method the maximum calculated pressure close to the focus shows some scattering depending on the grid size, random number generator, etc. Fig. 7 shows the pressure histories for a 90×90 grid. Figures 8 and 9 show examples for location 1 calculated with a 100×100 and a 75×75 grid, respectively. Of course, the solutions for the 100×100 grid are the best but there is no big difference with the 90×90 ver-

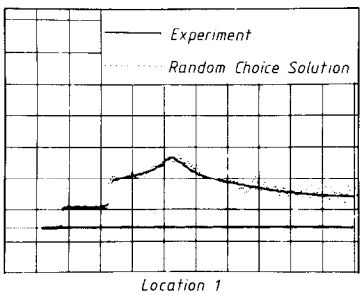

FIG. 8. Pressure history for a 100×100 mesh. Scales: 0.4 atm/division; 0.05 ms/division.

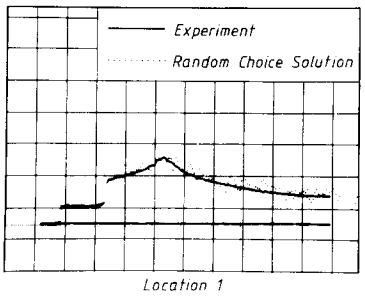

FIG. 9. Pressure history for a 75×75 mesh. Scales: 0.4 atm/division; 0.05 ms/division.

sion. So the convergence of the solution is very good using such a grid or a similar grid. One reason for the pressure fluctuations in the field behind the reflected shock is due to the stepwise approach of the reflector shape. Another reason is due to the error arising from the operator splitting technique (Colella (3)). These fluctuations are also seen in the pressure histories as scattering. However, the average of the numerical results agrees very well with the experimental ones. Figure 6 and also the pressure histories in Figs. 7–9 exhibit a certain waviness which adds to the random fluctuations. Though these waves have not been studied in detail so far, we have the impression that they show a similar qualitative behaviour as those similarly curved waves in Sturtevant's and Kulkarny's shadowgraphs (12, Fig. 3).

5.1.2. *Influence of the passive velocities.* In Section 3.1 the passive velocities are defined as those velocities which are normal to the computing direction, i.e., v and u are the passive velocities during an x and y sweep, respectively. Considering the first computation step, x sweep, one finds the solutions at grid points $((i+1/2)\,\Delta x, j\Delta x)$, see Fig. 5. Since the computation step was in the x direction, the solution at the grid points $((i+1/2\,\Delta x, j\Delta x)$ gives only u, the velocity in the x direction. In the second step, y sweep, one needs the velocities in the y direction at the grid points $((i+1/2\,\Delta x, j\Delta x)$ as initial conditions (Fig. 5). As mentioned before at these grid points only the velocities in the x direction are determined. There are several versions to determine the v components at the grid points $((i+1/2)\,\Delta x, j\Delta x)$. These v components are the passive velocities of the first step, x sweep. The same problems arise during the third and fourth step. Based on Chorin's concept, see (3.5), Colella (3) suggested determining the passive velocity dependent on the location of the contact surface and sampling point. If $x_* = u_* \Delta t$ indicates the location of the contact surface and x_i the position of the sampling point, then

$$v^{n\Delta t}_{(i+1/2)\,\Delta x, j\Delta x} = \begin{cases} v^{n\Delta t}_{(i+1)\,\Delta x, j\Delta x}, & x_i \geqslant x_* \\ v^{n\Delta t}_{i\Delta x, j\Delta x}, & x_i < x_*. \end{cases} \tag{5.1}$$

Equation (5.1) is valid for x sweeps. In y sweeps, v is to be replaced by u. This technique was used in all examples except that shown in Fig. 10. All calculations in

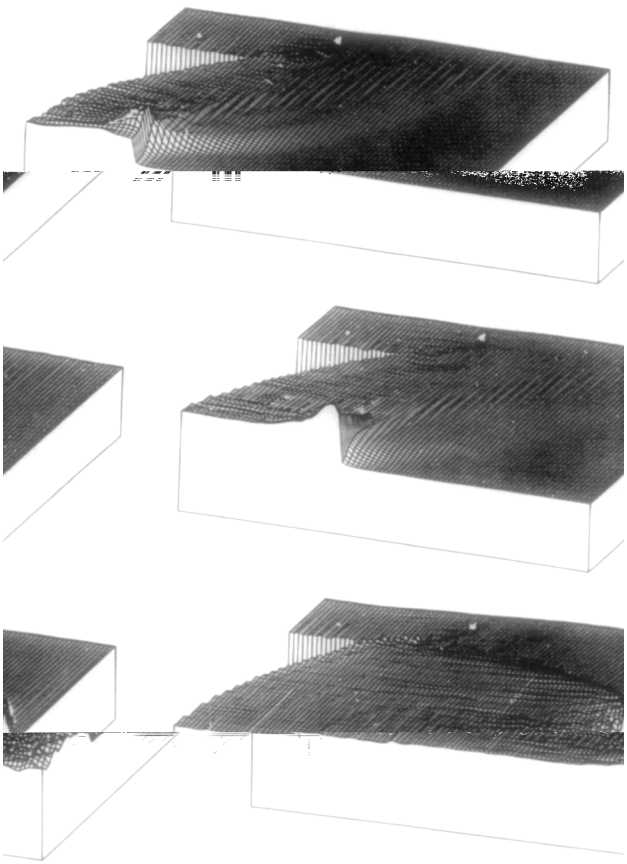

FIG. 10. Pressure field at several moments of focusing using (5.2) and (5.3).

this section are made with a 90×90 mesh to save computing time. A second technique determines the passive velocities by averaging. After the first step, x sweep, the velocities in the y direction at the grid points $((i+1/2)\,\Delta x, j\Delta x)$ are determined as follows:

$$v^n_{i+1/2,j} = \tfrac{1}{2}(v^n_{i+1,j} + v^n_{i,j}). \tag{5.2}$$

After the second step, y sweep, the velocities in x direction at the grid points $((i+1/2)\,\Delta x, (j+1/2)\,\Delta x)$ are determined in the following way (see Fig. 5)

$$u^n_{i+1/2,j+1/2} = \tfrac{1}{2}(u^n_{i+1/2,j+1} + u^n_{i+1/2,j}). \tag{5.3}$$

Because of the averaging a gentle smoothing occurs in contrast to the other technique (Fig. 10). Figure 11 shows the pressure histories for this version. As one sees the

pressure at the focus is not attenuated and broadened. Furthermore, the following rarefaction wave agrees well with the experiment. But at the other locations of the flow field the first method produces more accurate profiles (see Fig. 7). However, this example shows that due to (5.2) and (5.3) the fluctuations in the flow field are reduced effectively. Perhaps due to another weighted mean as in (5.2) and (5.3) the errors occurring in the pressure histories (Fig. 11) may be further reduced. But until this is found the first version described in this section seems to yield the best results (see Fig. 7).

5.1.3. *Influence of used random generators.* Figure 12a shows the pressure field which is obtained by the van der Coput generator with $k_1 = 2$ and $k_2 = 1$, shortened (2, 1). One sees that this generator produces numerical instabilities. These instabilities arise at the reflector boundary and sometime later they influence the whole flow field. Fig. 12b shows the same situation using the (2, 1) van der Corput generator, but now at all points where reflection occurs the sampling point $\theta \Delta x$ is set equal zero, i.e., the sampling point coincides exactly with the boundary (see Fig. 4). If the usual boundary conditions (2.8) are imposed and the sampling point occurs anywhere else than in the fan the state S_l or S_r represents the solution for the grid point $((i-1/2)\,\Delta x, (n+1/2)\,\Delta t)$ (see Fig. 4). This solution S_l or S_r may

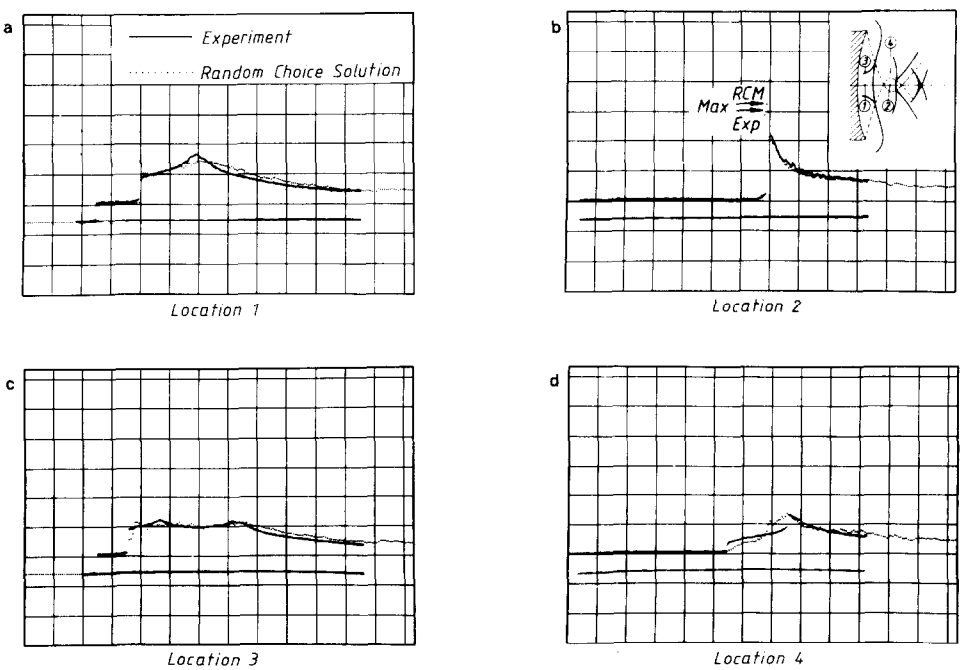

FIG. 11. Pressure histories obtained by using (5.2) and (5.3). Scales: 0.4 atm/division; 0.05 ms/division.

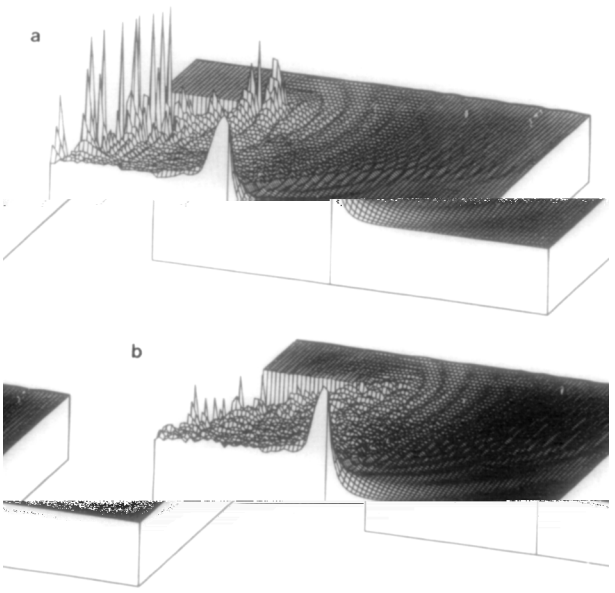

FIG. 12. Pressure field (a) using (2,1) van der Corput generator, (b) using (2, 1) van der Corpur generator with sampling point at the boundary ($\theta \cdot \Delta x = 0$).

yield a finite particle velocity u_l or u_r, i.e., at the boundary a finite particle velocity occurs. Physically this is not possible. If the sampling point $\theta \cdot \Delta x$ is set equal to zero at solid boundaries we always sample in the fan and the solution consists of state S_*. In this case the fluid velocity is u_* equal zero. Due to this procedure the instabilities are quite decreased as one notices comparing Figs. 12a and b. Although the instabilities could not be suppressed completely using the (2, 1) van der Corput generator the used procedure is an effective tool to improve the results obtained with other generators. In the one-dimensional case, however, using the same (2, 1) van der Corput generator the flow field is completely free of instabilities (Sommerfeld (10)).

Colella (4) proposed a van der Corput generator with (3, 2) for the x sweeps and with (5, 3) for the y sweeps. These generators were applied to obtain the results shown in Fig. 13. Without smoothing technique this combination produces instabilities similar to those of the (2, 1) van der Corput generator. In Fig. 13a the beginning of the instabilities can be seen. Figure 13b shows the pressure history at location 1. Using all tested van der Corput generators without smoothing technique in the two-dimensional shock focusing calculations no acceptable results could be obtained.

Contrary to Colella in the preceding examples only one random number for an x and y sweep was used and apparantly this procedure gives better results than Colella's technique. An obvious explanation for this assumption may be the

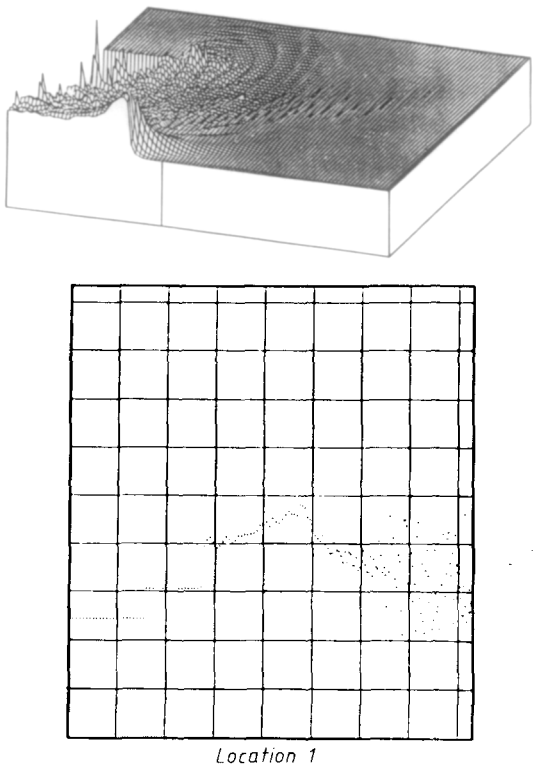

FIG. 13. Numerical results obtained by using van der Corput's (3, 2) and (5, 3) generators.

following. The propagation of a shock in the real flow field is approximated numerically by a propagation in the x and in the y direction. Of course, these two propagations in the x and y directions belong physically together. So they must have the same probability of propagation. This is ensured, when using the same random number for an x and y sweep.

Based on the preceding examples and other test calculations with different random generators it seems that the "chi-square" statistic (see Table I) has no important influence on the results. Chorin's generator with a relatively high "chi-square" statistic gives better results than the van der Corput generator with a "better" "chi-square" statistic.

The standard deviation alone is also no statistical quantity which allows a selection between good and bad generators. This can be seen from the following example. Table I shows that Chorin's generator with $m_1 = 2$, $m_2 = 3$, and $n_0 = 2$ has the smallest standard deviation with $\sigma = 16.17$. This generator was used with a 100×100 mesh, and Fig. 14 shows the obtained pressure history. The same example with the same mesh is shown in Fig. 8, where Chorin's generator with $m_1 = 3$, $m_2 = 7$, and $n_0 = 5$ is used. All other parameters are the same. Comparing the

pressure histories of Figs. 14 and 8 one finds that the first example with the larger standard deviation gives a better approximation to the experimental results than the example with the smallest standard deviation.

It is interesting to note that Chorin's generator with $m_1 = 3$, $m_2 = 7$, and $n_0 = 5$ gives the best arithmetical mean value and that this generator yields good results (see Figs. 7–9). It seems that the arithmetical mean value is a very important statistical quantity to find good generators, but certainly it is not the only one.

Until now it is not known which combination of statistical quantities has to be used to find the best random generator for two-dimensional problems. A further interesting point is that several random generators are good for calculations in one space dimension but produce instabilities in more than one space dimensions, like the (2, 1) van der Corput generator. This requires further investigations.

5.2. *Numerical Study of the Shape of a Diffracted Shock Wave*

In this section the diffraction of a shock wave at a 90° corner is considered. The results are obtained with the same method described in Section 3. Furthermore only one random number is used for both x and y sweep. These random numbers are obtained by Chorin's generator. Figure 15a shows the pressure distribution in a channel with the 90° branch. At the left end the pressure jump of the incident shock is seen. The incident shock runs from left to right. The cross section of the branch and the channel is approximated by 20 grid points. Figure 15b shows the pressure field after the shock has reached the branch.

One sees the diffracted shock which propagates into the branch and circular rarefaction waves propagating upstream. In this example the Mach number of the incident shock is $M_0 = 1.12$. In the next frame the diffracted shock has passed the opposite corner. A reflected shock propagates upstream. This reflected shock can be seen as a circular wave around the opposite corner. Because the area of the reflected shock increases continuously it is considerably attenuated. Thus in the next picture (Fig. 15d) it has already vanished. In Fig. 15d one sees also that the diffracted shock is almost parallel to the cross section of the branch.

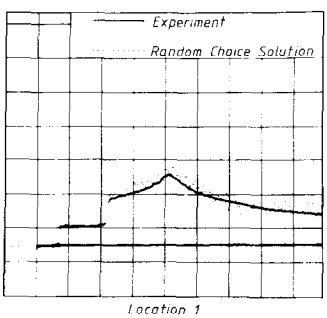

FIG. 14. Pressure histories obtained by using Chorin's generator with $m_1 = 2$, $m_2 = 3$, and $n_0 = 2$. Scales: 0.4 atm/division; 0,05 ms/division.

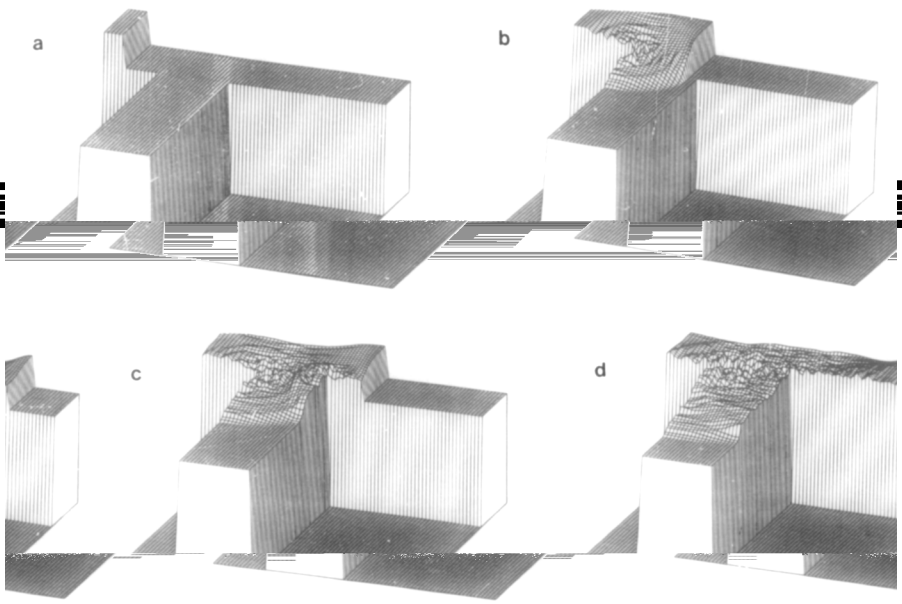

FIG. 15. Channel with a 90°-branch.

Figures 16a–d show the pressure distribution at several moments of diffraction. In Fig. 16e the diffracted pseudo-stationary shock wave profile is compared with the experimental one found by Skews (8). The Mach number of the incident shock wave is $M_0 = 1.2$. Calculations using the same method as described in Section 3 but keeping the passive velocities constant show a better agreement between experimental and numerical results as shown in Fig. 16e (6).

Figure 16e shows that in the numerical computation the diffracted shock is in general a little quicker than the experimental one. This is expected, since the numerical calculation does not include friction.

The scattering of the numerical results is due to several causes. First, as mentioned in Section 1, due to the randomness the shock position is not exact at any time, only the average position is. Furthermore, only 30 grid points are used to approximate the cross section of the channel and the branch. The error in the location of the shock position is of $0(\Delta x)$. Thus using more grid points the scattering of the numerical results can be reduced efficiently.

Colella (4) showed that due to the splitting technique errors arise. These errors become larger if the obliquity of the waves to the grid is increased. Of course the errors due to operator splitting are also increased keeping the obliquity constant and increasing the Mach number. These errors can be seen as numerical noise. To show the limit of computable Mach number to get acceptable results the next example shows the shock diffraction with an incident Mach number $M_0 = 1.5$.

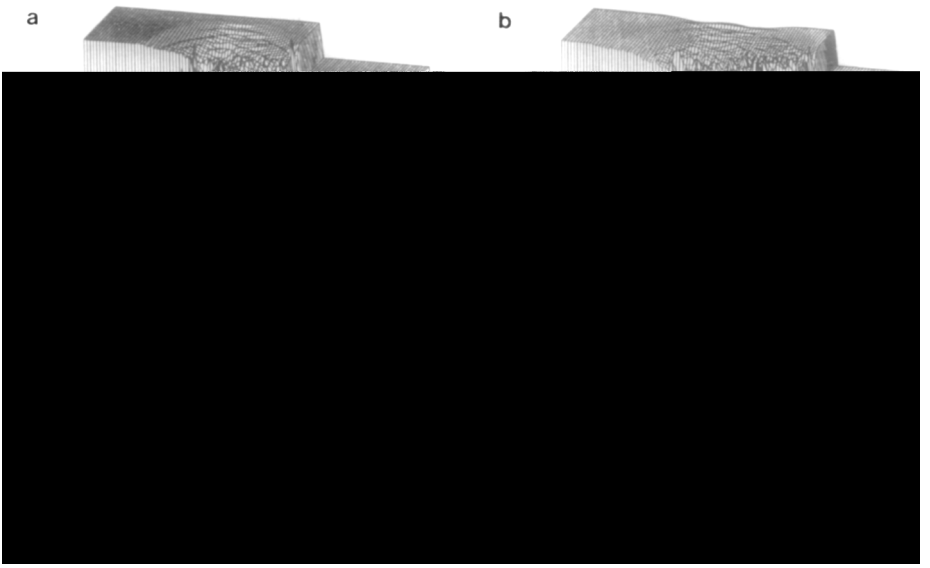

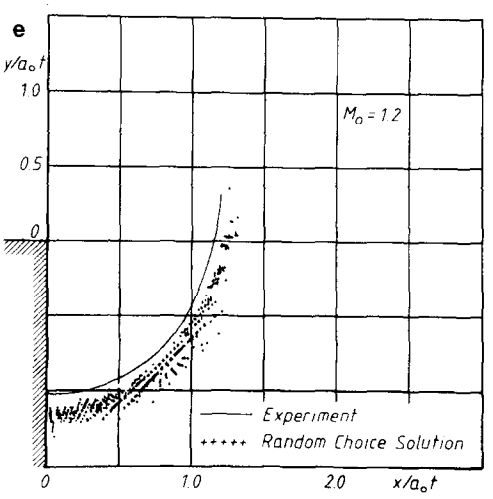

FIG. 16. Numerical example of shock diffraction.

Figures 17a and b show the pressure field of the diffraction problem. One sees that the noise is acceptable until the diffracted shock reflects at the opposite corner of the branch.

In Fig. 18 the comparison between the experimental and numerical pseudo-stationary shock wave profile can be seen. It is obviously that the agreement between the numerical and experimental results of Fig. 18 is comparable to, if not

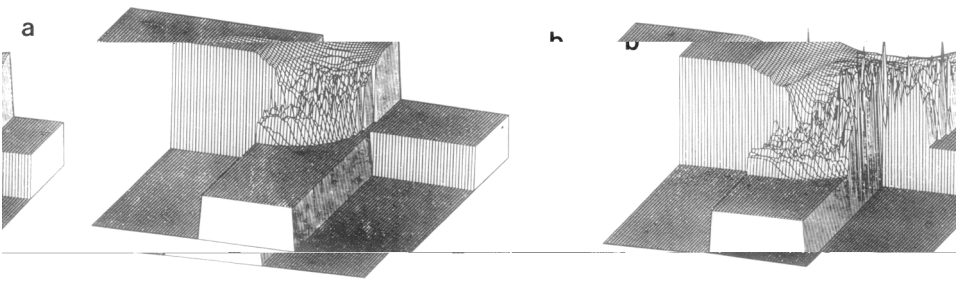

FIG. 17. Pressure field at several moments of diffraction, $M_0 = 1.5$.

somewhat better than, the results shown in Fig. 16e. This may be due to the following. If the incident Mach number is not big, the errors due to operator splitting cause a slight smearing of the diffracted shock (see Fig. 16). The noise is in this case not strong. Due to the slight smearing of the diffracted shock, the shock position is not exactly defined. Increasing the Mach number the noise becomes larger but the diffracted shock becomes steeper (see Fig. 17a), so the shock position of the diffracted shock is more exactly defined.

6. CONCLUSIONS

In this paper the behaviour of solutions obtained with the RCM is studied varying influential parameters of the method. The best results are yielded by using Chorin's random number generator. It is interesting to note that the random numbers produced by Chorin's generator are not as uniformly distributed as those

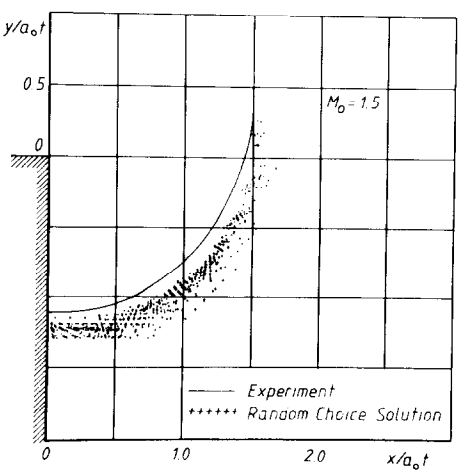

FIG. 18. Numerical and experimental pseudo-stationary shock wave profile.

obtained by van der Corput's generator. Furthermore the random numbers with the slowest standard deviation do not give the best numerical results, as it is shown in an example. Thus it seems, that none of these two statistical qualities can be used alone to choose a good random number generator for this field. Apparently a group of statistical qualities has to be considered together choosing a good generator. An explanation of this fact may be the following. In an one-dimensional RCM no errors arise due to the numerical method. Errors can only be induced by the choice of the random numbers. So the standard deviation is a sufficient tool to estimate the errors of the method. In a two-dimensional RCM which works with an operator splitting technique there is one group of errors due to the choice of the random numbers and another group of errors due to the splitting technique. So the standard deviation alone is not sufficient to choose good random numbers. Perhaps in future it may be possible to choose the random numbers in such a way, that the errors due to the splitting technique are reduced. With the present method it is not possible to compute flows with large Mach numbers, since the errors become unacceptable (see Sect. 5.2). The scattering of the results can be reduced effectively, if after every time step the solution is smoothed by averaging. This should be done only in the simple wave region to avoid the smoothing of discontinuities. However, due to this smoothing technique a physically existing waviness may be suppressed. Therefore in the preceding examples no smoothing technique was applied. An example of such a waviness can be seen in Fig. 6.

The RCM presented for two space dimensions can be extended to three-dimensional, rotational symmetrical flow. For example if the flow is rotational symmetrical to the x axis the results of the two-dimensional computation have to be modified by using the operator splitting technique for rotational symmetrical flow described by Saito and Glass (6) and other authors. Of course the method can be extended to arbitrary flows in three space dimensions but in the case of rotational symmetry no further mass storage is needed.

The typical computing time for the focusing problem is about 1800 sec CPU using a 90×90 mesh and running 200 time-steps. The example of the diffracted shock wave needs about 400 sec CPU running 100 time-steps. All calculations were done on a Cyber 175 computer.

ACKNOWLEDGMENTS

The research reported in this paper is part of a joint task conducted by the Sonderforschungsbereich 27 "Wellenfokussierung" supported by the Deutsche Forschungsgemeinschaft which is gratefully acknowledged.

REFERENCES

1. A. J. CHORIN, *J. Comput. Phys.* **22** (1976), 517.
2. A. J. CHORIN, *J. Comput. Phys.* **25** (1977), 253.

3. P. COLELLA, *Siam J. Sci. Stat. Comput.* **3** (1982), 76.
4. P. COLELLA, Lawrence Berkeley Laboratory, 1978.
5. J. GLIMM, *Comm. Pure Appl. Math.* **18** (1965), 697.
6. H. OLIVIER, Dissertation RWTH Aachen, 1985.
7. T. SAITO AND I. I. GLASS, UTIAS Report No. 240, 1979.
8. B. W. SKEWS, *J. Fluid Mech.* **29** (1967), 297.
9. G. A. SOD, *J. Fluid Mech.* **83** (1977), 795.
10. M. SOMMERFELD, Dissertation RWTH Aachen, 1984.
11. B. STURTEVANT, Private communication of July 5, 1983.
12. B. STURTEVANT AND V. A. KULKARNY, *J. Fluid Mch.* **73** (1976), 651.